Regional air pollution brightening reverses the greenhouse gases induced warming-elevation relationship

Zhenzhong Zeng, Anping Chen, Philippe Ciais, Yue Li, Laurent Li, Robert Vautard, Liming Zhou, Hui Yang, Mengtian Huang, Shilong Piao

AGU PUBLICATIONS

Geophysical Research Letters

RESEARCH LETTER
10.1002/2015GL064410

Key Points:
- Warming has been faster at higher-elevation stations globally
- The vertical gradient of warming rate varies with location
- Altitudinal differences in brightening modulate the warming-elevation gradient

Supporting Information:
- Figures S1–S20 and Table S1

Correspondence to:
S. Piao,
slpiao@pku.edu.cn

Citation:
Zeng, Z., A. Chen, P. Ciais, Y. Li, L. Z. X. Li, R. Vautard, L. Zhou, H. Yang, M. Huang, and S. Piao (2015), Regional air pollution brightening reverses the greenhouse gases induced warming-elevation relationship, *Geophys. Res. Lett.*, *42*, 4563–4572, doi:10.1002/2015GL064410.

Received 30 APR 2015
Accepted 21 MAY 2015
Accepted article online 26 MAY 2015
Published online 10 JUN 2015

Regional air pollution brightening reverses the greenhouse gases induced warming-elevation relationship

Zhenzhong Zeng[1], Anping Chen[2,3], Philippe Ciais[4], Yue Li[1], Laurent Z. X. Li[5], Robert Vautard[4], Liming Zhou[6], Hui Yang[1], Mengtian Huang[1], and Shilong Piao[1,7]

[1]Sino-French Institute for Earth System Science, College of Urban and Environmental Sciences, Peking University, Beijing, China, [2]Department of Ecology and Evolutionary Biology, Princeton University, Princeton, New Jersey, USA, [3]The Woods Hole Research Center, Falmouth, Massachusetts, USA, [4]Laboratoire des Sciences du Climat et de l'Environnement, Gif sur Yvette, France, [5]Laboratoire de Météorologie Dynamique, Centre National de la Recherche Scientifique, Université Pierre et Marie Curie-Paris 6, Paris, France, [6]Department of Atmospheric and Environmental Sciences, University at Albany, Albany, New York, USA, [7]Institute of Tibetan Plateau Research, Chinese Academy of Sciences, Beijing, China

Abstract Mountain waters, glaciers, hazards, and biodiversity are vulnerable to the impacts of global warming. Warming is projected to amplify over mountains by global climate models, yet meteorological records do not show a uniform acceleration of warming with elevation. Here we explore warming-elevation relationships using records from 2660 meteorological stations and determine that the vertical gradient of warming rate varies with location. The warming is faster at higher altitudes in Asia and western North America, but the opposite is observed over Central Europe and eastern North America which have received more short-wave radiation (brightening) associated with a decrease of aerosols and clouds since the 1980s. We found that altitudinal differences in air pollution (brightening), with observations showing more short-wave radiation received at low altitudes than at mountains, modulate the warming-elevation relationships. The advance in understanding of the drivers of regional climate change will contribute to the formulation of strategies for climate change mitigation at high elevations.

1. Introduction

Land surface air temperature has warmed by 0.9 ± 0.2°C between 1979 and 2012 [*Hansen et al.*, 2006; *Stocker et al.*, 2013]. Global climate models (GCMs) predict a rather uniform faster warming trend at higher elevations as a consequence of increasing greenhouse gases (GHGs) [*Giorgi et al.*, 1997; *Fyfe and Flato,* 1999; *Santer et al.*, 2005; *Kotlarski et al.*, 2012; *Rangwala et al.*, 2013; *Stocker et al.*, 2013]. However, meteorological records do not show a uniform acceleration of warming with elevation [e.g., *Beniston et al.*, 1997; *Pepin and Lundquist*, 2008; *Rangwala and Miller*, 2012]. Positive [e.g., *Beniston and Rebetez*, 1996; *Liu et al.*, 2009; *Wang et al.*, 2013], nonsignificant [e.g., *Pepin and Lundquist*, 2008; *You et al.*, 2010] or negative [e.g., *Vuille and Bradley*, 2000; *Lu et al.*, 2010] correlations between air temperature trends and elevation have been diagnosed from station data. This inconsistency between model prediction and in situ observations raises the question about the ability of current climate models to accurately describe regional climate change patterns.

With GHG forcing being the dominant driver of air temperature warming [*Stocker et al.*, 2013], feedbacks in the climate system and short-lived forcing agents such as aerosols could strongly modulate the rate of change of temperature with time, across regions and at altitude. The observed spatial structure of the differences between surface station observations and model predictions can provide indications about mechanisms not captured by models, such as trends in cloudiness and aerosols which change the radiative forcing of the surface, and lengthening growing seasons in mountain regions that may both decrease albedo and increase local cooling from plant transpiration.

Here we use a large data set of meteorological station data to document the relationship between air temperature trends and elevation in the Northern Hemisphere (NH) during the last 30 years. We collected data from 2660 meteorological stations across the NH, with continuous records of mean temperature, maximum temperature (a proxy of daytime temperature), and minimum temperature (a proxy of nighttime temperature) between 1982 and 2010. The goals of the study are to detect regions with positive or negative correlations between warming and elevation, and to discuss plausible mechanisms that can explain the sign of these regional correlations.

2. Materials and Methods

2.1. Meteorological Observation Data

The data set of meteorological station observations has been retrieved from the Global Surface Summary of the Day collection archived at the National Climatic Data Center (GSOD; ftp://ftp.ncdc.noaa.gov/pub/data/qsod), the Monthly Surface Climate Variables of China catalog derived from the National Meteorological Information Center of the China Meteorological Administration (CMA; http://cdc.cma.gov.cn), and the Global Historical Climate Network Monthly Version 3 (GHCN) [*Lawrimore et al.*, 2011]. GSOD provided meteorological observations from data exchanged under the World Meteorological Organization World Weather Water Program, including 26,247 weather stations located around the world with meteorological records generally from 1929 to the present. After removing stations that have missing measurements for more than 1 month during the study period (1982 to 2010), there were 2235 GSOD meteorological observation stations over the Northern Hemisphere selected for this study. In addition, there are 728 CMA stations distributed across China. Most of these station observations are continuous over the period from 1951 to the present. After excluding those stations with discontinuous measurements or which duplicate the 2235 stations in GSOD (see above), we obtained another 266 meteorological stations from CMA. Similarly, we also obtained 159 meteorological stations form GHCN, mainly distributed over America. In total, data from 2660 meteorological observation stations were used in this study, each yielding continuous monthly records of mean temperature, maximum temperature, and minimum temperature for 1982 to 2010. The monthly temperatures (mean, maximum, and minimum) are the averages of daily values during each month, which are based on the hours of operation for each station.

All the monthly mean temperature data for the 2660 stations were extracted from three data sets (GSOD, CMA, and GHCN), which have undergone extensive automated quality control to eliminate random and systematic errors, including inhomogeneity caused by factors such as station relocations, changes in instrumentation, and environmental changes. These three input data sets are of high quality and have been widely used to study climate change [e.g., *Wang et al.*, 2009]. Figure S1 in the supporting information shows the distribution of these stations, which are densely distributed in America, Europe, and East Asia (China, South Korea, and Japan). The elevations of the stations range from 0.3 m to 4900 m. More than 24% of the stations are distributed in high-elevation areas (altitudes higher than 500 m above sea level (asl)).

2.2. Data Analyses

The warming rate was calculated using least squares linear regression for the period of 1982–2010. At the hemispheric scale and in large mountain regions, we compared the warming rate with elevation to assess whether there is an elevation dependency of warming rate at these scales and regions. We define three large mountain regions: the Rocky Mountains and surroundings (125°W–95°W, 30°N–60°N, Rockies hereafter), the Alps and surroundings (4°E–20°E, 40°N–52°N, Alps hereafter), and the Himalaya and Tibetan Plateau, and its surroundings (73°E–122°E, 20°N–55°N, HTP hereafter). These three regions include 82% of all the mountain stations (≥500 m asl) in the NH and have a better representativeness than smaller massifs where temperature can be influenced by local effects and the small number of stations [*Pepin and Lundquist*, 2008]. In addition to the mean temperature trend, we also assessed trends in daytime maximum temperature and nighttime minimum temperature, because both the rate and processes of daytime warming differ from those of nighttime warming.

At a local scale, the altitude gradient of warming rate was estimated using a regional pair-based robust multiple linear regression. We included longitude and latitude in the multiple linear regression to exclude the influence of continentality and latitude [*Li et al.*, 2013]. Extreme warming at a specific station might strongly affect the ordinary least squares linear regression and could result in an unreasonable gradient. To reduce the impact of extreme temperature trends at some stations, robust regression [*Rousseeuw and Leroy*, 2005] rather than least squares linear regression was used in this study. Finally, the altitude gradient at a station was estimated for the station and its adjacent 50 stations using the robust multiple linear regression shown by equation (1).

$$Y = k_0 + k_1\mathrm{Elev} + k_2\mathrm{Lat} + k_3\mathrm{Lon} \quad (1)$$

where Y is warming rate; Elev, Lat, and Lon are elevation, latitude, and longitude at each station; and k_0, k_1, k_2, and k_3 are the regression coefficients, respectively. The coefficient k_1 is the altitude gradient.

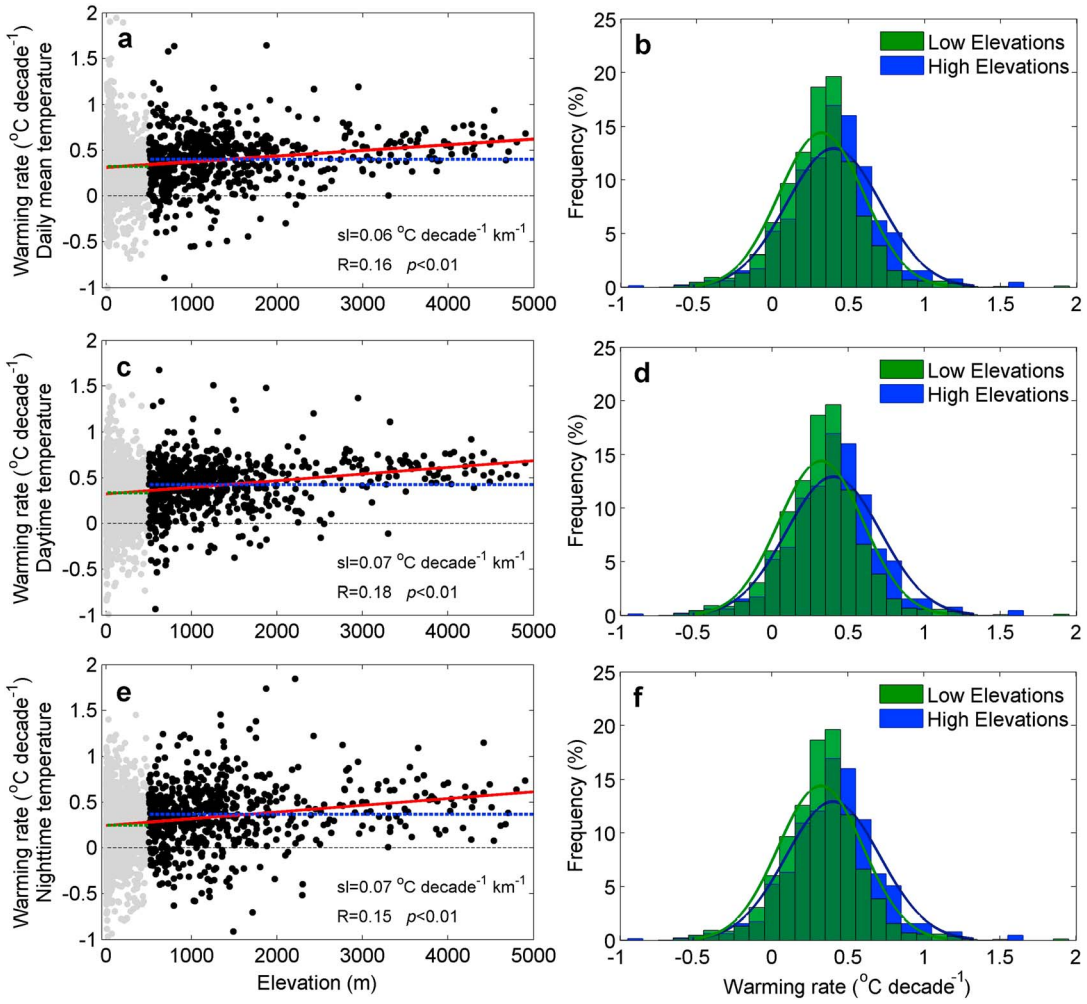

Figure 1. Global relationship between elevation and warming rate (1982–2010: °C decade^{-1}) for 2660 meteorological stations: (a, b) daily mean warming, (c, d) daytime warming, and (e, f) nighttime warming. (a, c, and e) Scatterplots of warming rate versus elevation. The green and blue horizontal dashed lines represent the average warming rate for the low-elevation (<500 m asl) stations and the high-elevation (≥500 m asl) stations, respectively; the red line is a fit line between warming rate and elevation. (b, d, and f) The probability distribution of warming rate at low-elevation stations (green) and high-elevation stations (blue), respectively.

3. Results and Discussions

3.1. Global Warming-Elevation Relationships

We first analyze differences in temperature trends with altitude using the data from 2660 stations (Figure 1). More than 1616 stations show a significant ($p < 0.05$) warming trend since the 1980s (Figure S2) [*Hansen et al.*, 2006; *Stocker et al.*, 2013]. The magnitude of the warming trend ($\dot{T}$) increases with increasing elevation (Z), defining a warming rate vertical gradient ($\partial \dot{T}/\partial Z$) of 0.06 ± 0.008°C decade^{-1} km^{-1} ($p < 0.01$; Figure 1a). The average temperature trend of mountain stations (0.40°C decade^{-1} for stations more than 500 m asl) is higher than that of lowland stations (0.32°C decade^{-1} for stations below 500 m asl). The difference between mountain and lowland warming rates is significant ($p < 0.01$ with two-sample t test). The fact that the statistical distribution of warming rates versus altitude is positively skewed (Figure 1b) further indicates that warming rate is larger at the higher elevation sites. Similar results are also found for trends of daytime (Figures 1c and 1d) and of nighttime warming (Figures 1e and 1f).

3.2. Regional Differences in the Warming-Elevation Relationships

We characterize regional differences in the $\dot{T}$-Z relationship using two statistical methods. In the first method, $\dot{T}$-Z regression analysis was performed separately for each large mountain region (Figure 2). With this first method, warming rates are found to increase with altitude over the Rockies and the HTP (Figures 2b and 2d).

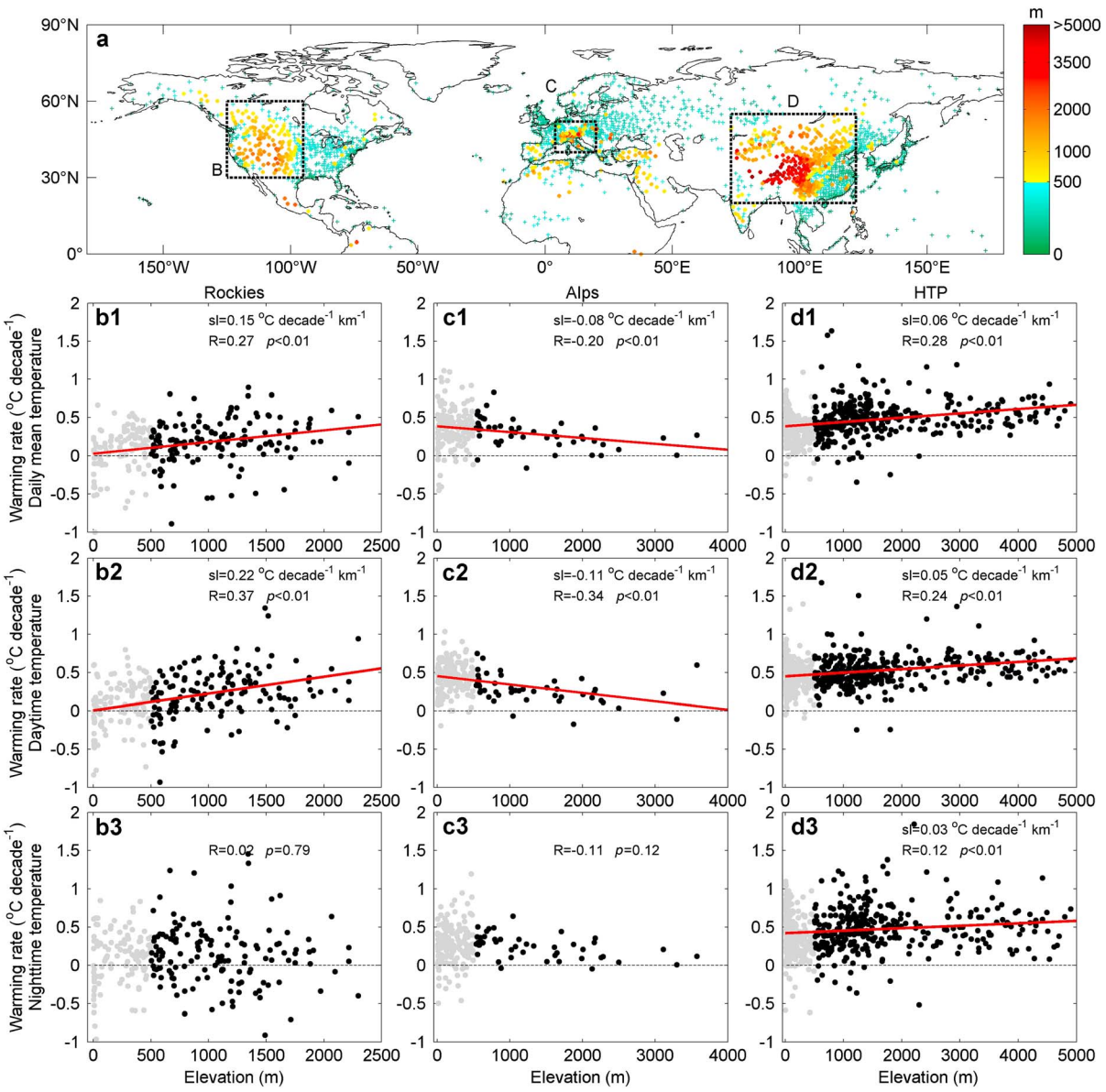

Figure 2. Warming-elevation relation in the three largest mountain regions. (a) Elevations of the 2660 meteorological stations. Most high elevation (≥500 m asl) stations are distributed in the (b1–b3) Rockies, the (c1–c3) Alps, the (d1–d3) Tibetan Plateau and their surroundings. Warming-elevation relationships for all the stations in these mountain regions: (b1, c1, and d1) daily mean warming, (b2, c2, and d2) daytime warming, and (b3, c3 and d3) nighttime warming.

But in the Alps, the opposite is observed (Figure 2c), suggesting different mechanisms over the Alps. Daytime and nighttime temperatures also show regional differences in $\dot{T}$-Z relationships (Figures 2b2–2d3). The sign of the regression slope of daytime $\dot{T}$-Z is similar to that of daily mean $\dot{T}$-Z, with a positive elevation dependence around the Rockies and the HTP, but a negative one around the Alps. On the other hand, nighttime warming is only weakly correlated with altitude (Figures 2d2 and 2d3). Nonsignificant nighttime $\dot{T}$-Z correlations are found in the Rockies and the Alps. In the Rockies region, the trend of annual snow/ice-covered days is negative at most stations (63%, Figure S3a). The number of snow-covered days in the Rockies also decreases faster with increasing altitude (-2.5 ± 0.8 days decade^{-1} km^{-1}, $p < 0.01$; Figure S3b). The different dependency of daytime and nighttime warming upon elevation is qualitatively consistent with the positive regional feedbacks caused by decreased albedo resulting from the reduction in snow and ice cover in mountainous regions [*Giorgi et al.*, 1997; *Pepin and Lundquist*, 2008; *Rangwala and Miller*, 2012]. In the Alps, the trend in snow-covered days also decreases with increasing altitude

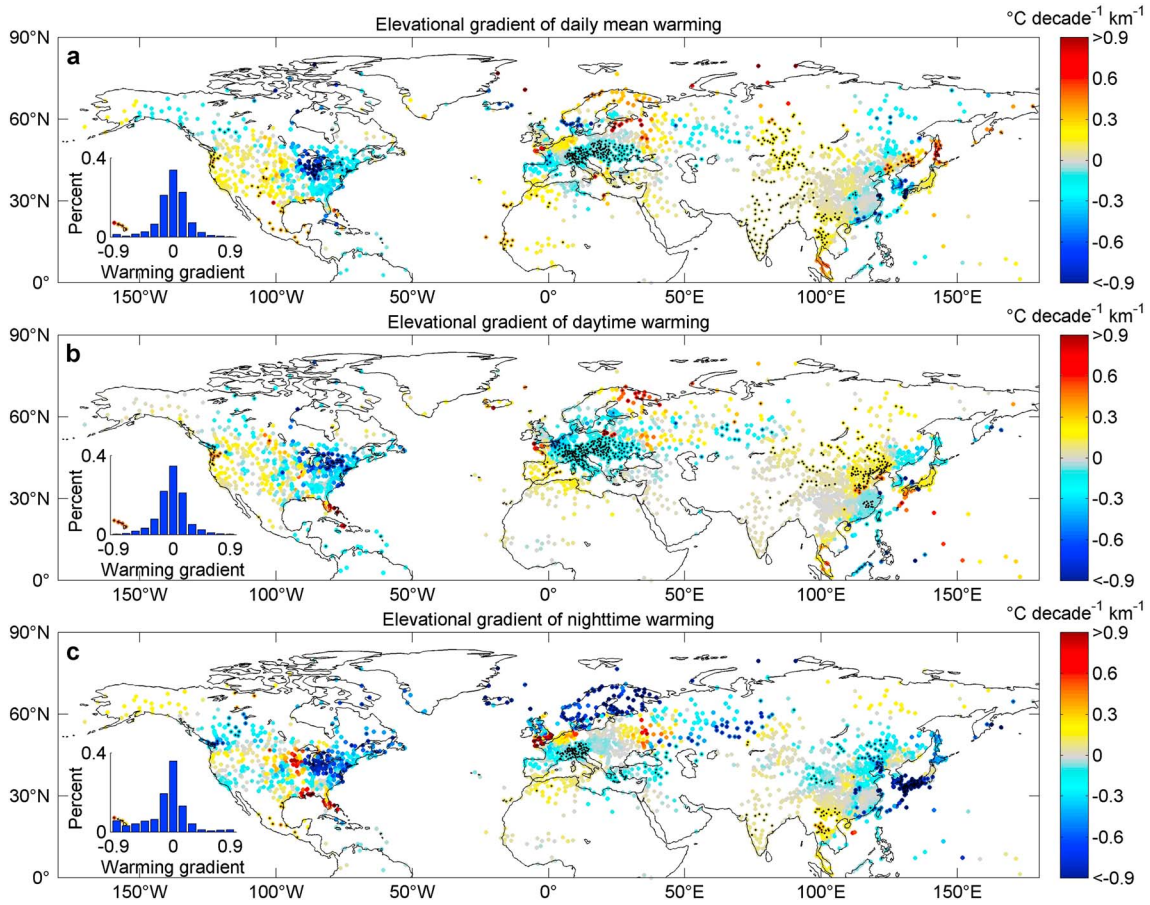

Figure 3. Spatial distributions of elevational gradient in (a) daily mean warming, (b) daytime warming, and (c) nighttime warming. The regional gradient of warming rate against elevation is quantified using a robust multiple linear regression for the station and its neighboring 50 stations. Black dots show a significant relationship ($p < 0.05$). The insets show the histogram distribution of the gradients of warming rate against elevation.

(-2.7 ± 1.2 days decade^{-1} km^{-1}, $p < 0.05$; Figure S3d), but the warming gradient with elevation is negative (Figures 2b1–2b3), further suggesting that other mechanisms are involved in the Alps, such as altitudinal differences of increased short-wave brightening due to reduced aerosol loading.

In the second method to characterize regional $\dot{T}$-Z relationships, we used pairs of neighboring stations at different altitudes and calculated an average $\dot{T}$-Z gradient from a regional pair-based robust multiple linear regression (see section 2). Fifty-three percent of the station pairs show a positive $\dot{T}$-Z correlation, and the rest have a negative correlation (Figure 3a), which illustrates the strong spatial heterogeneity. Regionally, these correlations are either dominantly positive or dominantly negative (Figure 3a and Table S1). Consistent with the first method, we found positive $\partial\dot{T}/\partial Z$ in the Rockies (0.09°C decade^{-1} km^{-1}) and HTP (0.02°C decade^{-1} km^{-1}), and negative $\partial\dot{T}/\partial Z$ in the Alps (-0.06°C decade^{-1} km^{-1}). The spatial pattern of the vertical gradient $\partial\dot{T}/\partial Z$ is similar for daytime and daily mean temperatures (Figure 3b). Figures 3a and 3b show positive $\partial\dot{T}/\partial Z$ values over mountains and high plateaus (western North America, Mexico, and Asian high plateaus), over some areas of northeastern Europe and the North China Plains, confirming positive $\partial\dot{T}/\partial Z$ as indicated by previous studies [e.g., *Fyfe and Flato*, 1999; *Liu et al.*, 2009]. Negative $\partial\dot{T}/\partial Z$, i.e., a faster warming of lowland stations or a slower warming of mountain stations are found in eastern North America (around the Great Lakes), Central Europe, Korea, and Southern China (around the Pearl River and Yangtze River Delta regions).

The spatial pattern of nighttime $\partial\dot{T}/\partial Z$ gradient using the pair regression approach (Figure 3c) is different from that of daytime $\partial\dot{T}/\partial Z$ (Figure 3b). Compared to the daytime $\dot{T}$-Z correlation, the nighttime $\dot{T}$-Z correlation is weaker and noisier across the three mountain ranges (Figure 3c), similar to results obtained with the first method (Figure 2). Globally, there are more negative correlations at nighttime than daytime (Figures 3b and 3c,

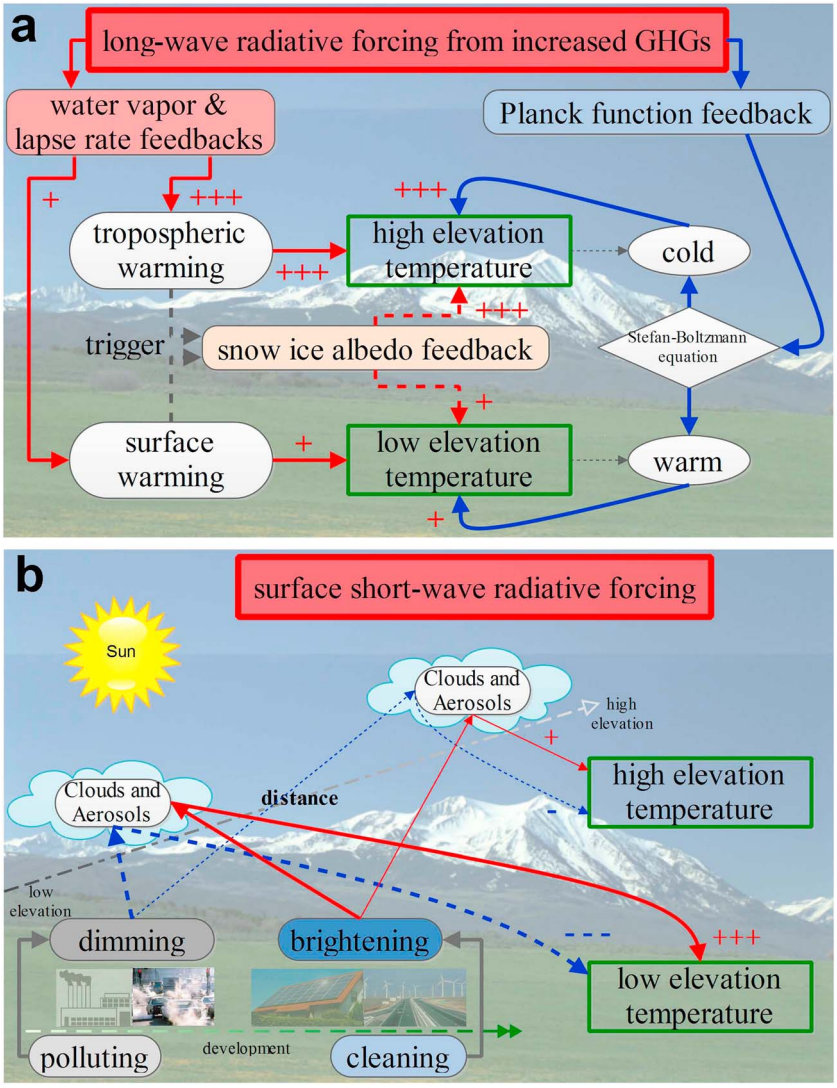

Figure 4. Schematic of plausible mechanisms for the warming-elevation relationship. Conceptual diagrams for warming-elevation relationship induced by (a) greenhouse gases forcing and (b) changes in atmospheric aerosols and clouds. Red (blue) lines show positive (negative) radiative feedbacks. The signs "+" and "−" represent increasing and decreasing local temperature, respectively. The number of the signs indicates the magnitude of the effects.

see histogram distribution in inset). The negative correlations are mostly distributed over lowland areas with denser populations, higher pollution, and stronger urban heat island effects (using as proxy, the satellite derived night light index (NLI) [*Elvidge et al.*, 2009], Figure S4), such as Eastern America, California, Europe, and East Asia (Figures 3c and S4b). Interestingly, we found that the area with negative daytime $\dot{T}$-Z correlation over Central Europe shows a large decrease from daytime to nighttime; while over the North China Plain, widespread positive daytime $\dot{T}$-Z correlation changes into negative at night (Figures 3b and 3c). The results of regional gradient of warming rate against elevation (Figure 3) are also robust regardless of the choice of regression method (Figure S5) and the choice of parameters within the regression (Figure S6).

In summary, we determine a significant positive $\dot{T}$-Z correlation around the Rockies and the HTP, and a significant negative $\dot{T}$-Z correlation over Central Europe (including the Alps; Figure S7) and northeastern United States (Figure S8).

3.3. Mechanisms Driving the Warming-Elevation Relationships

Several mechanisms support that the greenhouse gases induced warming-elevation relationship should be positive. First, the long-wave forcing from increased GHGs implies faster warming in the troposphere than at

the surface (Figure 4a, solid red line) [*Douglass et al.*, 2004; *Santer et al.*, 2005; *Stocker et al.*, 2013], and this fingerprint should logically be detected at mountain stations [*Pepin and Losleben*, 2002; *Pepin and Lundquist*, 2008; *Rangwala and Miller*, 2012]. Second, the tropospheric warming over mountains can also trigger local positive snow/ice albedo feedbacks that can increase the positive value of $\partial \dot{T}/\partial Z$, which is qualitatively consistent with a stronger snow/ice albedo feedback in mountain regions that have more snow, and therefore more snow to lose in response to warming (Figure 4a, dashed red line) [*Beniston et al.*, 1997; *Pepin and Lundquist*, 2008; *Rangwala and Miller*, 2012; *Rangwala et al.*, 2013; *Wang et al.*, 2013]. Additionally, the total radiation emitted by the land surface is proportional to the fourth power of land surface temperature. Thus, for the same GHG forcing, the increase of radiative emissions (and thus surface temperature), to keep energy balance, should be larger in mountains than in lowland areas due to lower skin temperature [*Ohmura*, 2012] (Figure 4a, blue line). As a result, warming should be faster at altitude from the GHG forcing (Figure 4a). This theory is verified by global climate model projections (e.g., Coupled Model Intercomparison Project Phase 5) [*Rangwala et al.*, 2013] and regional climate model simulations under elevated GHGs [*Giorgi et al.*, 1997; *Fyfe and Flato*, 1999; *Liu et al.*, 2009; *Kotlarski et al.*, 2012]. Thus, both the global positive $\dot{T}$-Z correlation and the regional positive $\dot{T}$-Z correlation over the Rockies and the HTP regions are consistent with the GHG forcing.

The prevailing significant negative $\dot{T}$-Z relationship over Central Europe and northeastern United States led us to ask which factors modify the GHG induced warming-elevation relationship over these regions. To address this question, we postulate that lowland Central Europe and northeastern United States are receiving more short-wave surface forcing due to decreasing aerosols and clouds and have thus warmed faster than mountains (Figure 4b). This mechanism assumes that (1) the increased short-wave forcing (the so-called brightening effect) [*Wild et al.*, 2005; *Wild*, 2012], due to decreases in aerosols and clouds, occurs in Central Europe and northeastern United States, and that (2) the increasing short-wave forcing primarily acts to increase lowland temperatures (i.e., stronger brightening effects in lowland regions than high altitudes) (Figure 4b, solid red lines).

An acceleration of surface warming by an increase in the short-wave forcing of the surface has been hypothesized [*Vestreng et al.*, 2007; *Wang and Dickinson*, 2013] (Figure 4b, solid red lines). Both brightening and dimming (the opposite effects of decreasing short-wave radiation) are primarily determined by trends in aerosols and clouds [*Wild et al.*, 2005; *Ruckstuhl et al.*, 2008; *Wang and Dickinson*, 2013]. Brightening has been documented over North America and Europe, where air quality has improved in recent decades [*Wild et al.*, 2005; *Vestreng et al.*, 2007; *Wild*, 2012; *Wang and Dickinson*, 2013]. We further verify that trends in surface short-wave radiation are positive at most American and European stations (brightening) but negative in East Asia (dimming) (Figure 5a). Thus, both literature and observations support the first condition for negative $\partial \dot{T}/\partial Z$ values in the mechanism: negative $\partial \dot{T}/\partial Z$ is associated with areas where aerosols and clouds have decreased.

This is not enough, however, since decreasing clouds and aerosols can warm mountains as well as lowlands. Thus, a second condition is that aerosols and clouds have decreased *more* at lowland stations than at mountain stations, or in other words that brightening is more pronounced over lowland areas (Figure 4b). This condition is likely to be met over developed regions because (1) most aerosol and cloud trends derive from changes in emissions of air pollutants in lowland areas, and the trends should attenuate with increasing distance from the pollution sources [*Vautard et al.*, 2009], and (2) aerosol concentrations at high elevation are inherently low, so that their influences on the temperature trends are less in mountainous areas [*Ruckstuhl et al.*, 2008; *Philipona*, 2013]. Hence, we expect a negative elevational gradient of brightening to explain the negative $\partial \dot{T}/\partial Z$ values in Central Europe and northeastern United States.

To test for this condition, we analyzed regional elevational gradients of trends in aerosols and clouds. In Central Europe, several long-term observations support the idea that the magnitude of decreasing aerosols has decreased with altitude. First, both the trends in the meteorological visibility inverse and the number of days with visibility <5 km are negative (Figures S9 and S10) [*Wang et al.*, 2009], confirming decreasing aerosols in Central Europe [*Ruckstuhl et al.*, 2008; *Vautard et al.*, 2009; *Wang and Dickinson*, 2013]; and the magnitudes of these trends decrease with altitude (Figures 5b and S11–S13). Second, the incoming short-wave radiation trend significantly decreases with elevation (Figures 5c and S14), while cloud fraction trends are weakly correlated with elevation (Figures 5d and S15), indicating a

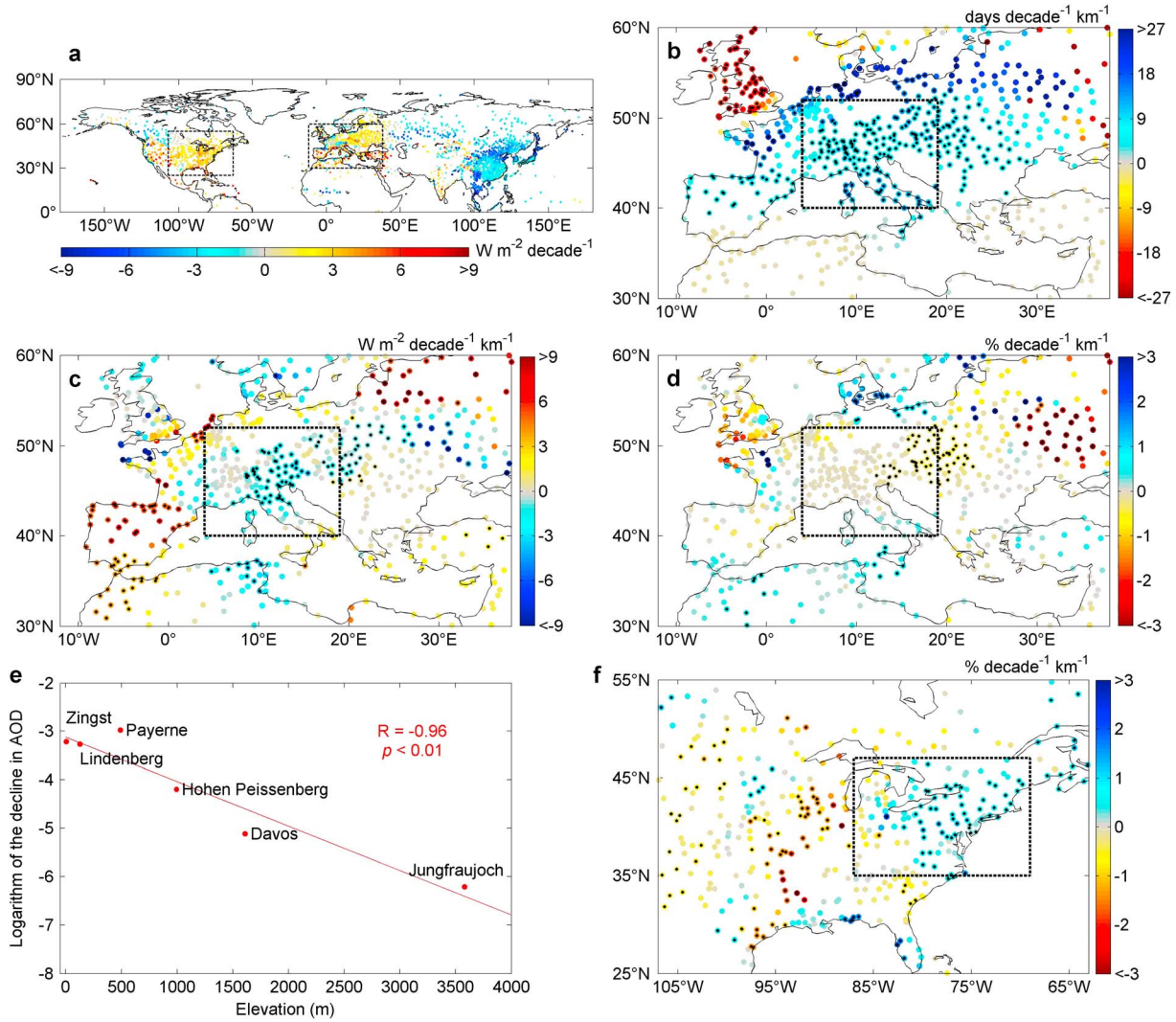

Figure 5. Regional differences in the global warming-elevation relationship induced by greenhouse gases as modified by atmospheric aerosol and cloud changes. (a) Trend in incoming surface radiation (1984–2007: W m^{-2} decade^{-1}). Gradients of (b) the trend of number of days with visibility <5 km (1982–2010; days decade^{-1}), (c) the incoming surface radiation trend (1984–2007: W m^{-2} decade^{-1}), and (d) the cloud fraction trend (1982–2010: % decade^{-1}) against elevation over Central Europe. (e) Logarithm of the decline in AOD (1995–2005: per decade) versus elevation for six AOD observation sites in Central Europe (37). (f) Gradient of cloud fraction trend against elevation over eastern North America. For Figures 5a and 5c, annual surface radiation at each station is extracted from the station-located-pixel (1° × 1°) values from the NASA/Global Energy and Water Cycle Experiment Surface Radiation Budget Release-3.0 data set. For Figure 5b, the meteorological station observations of visibility are collected from GSOD. For Figures 5d and 5f, the annual cloud fraction at each station is extracted from the station-located-pixel (0.5° × 0.5°) values from the Climatic Research Unit TS 3.21 data [*Harris et al.*, 2014]. For Figures 5b–5d and 5f, the regional gradient at each station is quantified using a robust multiple linear regression for the station and its neighboring 50 stations. For Figures 5b–5d and 5f, dashed boxes indicate the regions with significant negative correlation between warming and elevation. Warm colors are used to indicate a warming effect, and cold colors to indicate a cooling effect, respectively. Dotting represents a significant elevational gradient ($p < 0.05$).

negative gradient of the decline in aerosols against elevation. Additionally, a few long-term surface measurements of aerosol optical depth (AOD) in Central Europe further verify the negative elevational gradient of the temporal decline in aerosols: the logarithm of the decline in AOD at each site (1995–2005) significantly decreases with elevation ($R = -0.96$, $p < 0.01$; Figure 5e) [*Ruckstuhl et al.*, 2008; *Philipona*, 2013]. This is in line with the fact that faster warming over Europe compared to other regions is partly caused by increasing short-wave radiation, possibly due to improved air quality and aerosol decrease as well as to the observed decline in fog, mist, and haze [*Wild et al.*, 2005; *Vestreng et al.*, 2007; *Ruckstuhl et al.*, 2008; *Streets et al.*, 2009; *Vautard et al.*, 2009]. In eastern North America, the brightening is attributed to the decreasing trend in cloudiness [*Augustine and Dutton*, 2013; *Wang and Dickinson*, 2013], and we suppose that it is altitudinal difference in cloudiness trend that leads to the

significant negative $\dot{T}$-Z correlation over the region. The decreasing trend in cloudiness is partly due to the improved air quality after the 1970 Clean Air Act Amendments in the United States [*Dominici et al.*, 2007] (Figure S16) through the indirect effect of aerosols (i.e., acting as cloud condensation and ice nuclei). Assuming that air pollution was more serious before the implementation of stricter air quality control measures over more densely populated regions, we expect elevational differences in air quality improvement according to the significantly negative gradients of NLI against elevation in the northeastern United States (Figure S4c); and in fact, we do find a positive elevational gradient of the cloud fraction trend (Figures 5f and S17). Thus, both conditions for elevational gradient of brightening are met over the northeastern United States (Figures 5f, S4c, S16, and S17), which explains the observed, although mostly insignificant, negative gradient of daytime warming against elevation over the region (Figures 3b and S8). Although there is a reduction in aerosol over the southeastern United States (Figure S16), the elevational gradients of warming are not significant over this region (Figure 3b) because of the lack of significantly negative gradient of NLI against elevation (Figure S4c, second condition not met).

Last but not least, dimming due to increasing aerosols and deteriorating air quality in the North China Plain [*Xia*, 2010] is also qualitatively consistent with the cooccurrence of positive daytime $\dot{T}$-Z correlations (Figures 3b and S18) and negative nighttime $\dot{T}$-Z correlations (Figures 3c and S19) in that region. Increasing black carbon aerosols in particular has the property to dampen daytime warming but increases nighttime warming over polluted lowland regions. The same mechanism also possibly explains the positive warming-elevation gradient in India (Figure 3), where black carbon emissions have drastically increased during the past three decades [*Menon et al.*, 2002]. In addition, our data analysis shows that the two conditions for elevational gradient of brightening are not met in the Rockies and HTP (Figure S20); thus, this mechanism (Figure 4b) does not change the positive warming-elevation correlations induced by increasing GHGs (Figure 4a) over these regions (Figures 2 and 3).

4. Conclusions

Our results indicate that the warming-elevation relationship differs from regions, and quantifying the elevation-warming relationship can help to test hypotheses on mechanisms and feedbacks that matter in regional climate change. Here warming amplification at higher latitudes due to GHG forcing predicted by GCMs [e.g., *Beniston et al.*, 1997; *Giorgi et al.*, 1997; *Fyfe and Flato*, 1999; *Rangwala et al.*, 2013; *Wang et al.*, 2013] is verified at the hemispheric scale and for some large mountain regions. However, negative gradients of daytime warming against elevation since the 1980s are found over Central Europe and eastern North America. This observation is consistent with the role played by variations in short-wave radiation that may be due to changes in both atmospheric aerosols and clouds [*Wang and Dickinson*, 2013], and confirms that trends in air quality (i.e., aerosol emissions) have remarkably affected regional temperature changes over the last three decades [e.g., *Ruckstuhl et al.*, 2008; *Vautard et al.*, 2009]. Therefore, the inconsistency between model prediction and in situ observations highlights the importance of accurate descriptions of atmospheric aerosol and cloud processes in climate models for the improvement of climate predictions. These improved predictions will contribute to the formulation of strategies for climate change mitigation, such as biodiversity conservation at higher elevations where the fate of species is more vulnerable to climate change [*Inouye et al.*, 2000; *Field et al.*, 2014].

We realize that a high correlation does not imply causality. Our attribution of short-wave radiation trends to the changes in aerosols and clouds is still preliminary, given that decadal modes of climate variability can also change atmospheric transport, aerosol content, and the frequency of cloudy days. The contribution of regional brightening and dimming to regional $\dot{T}$-Z gradients remains highly speculative because of the lack of detailed long-term observations of aerosols and cloudiness. Thus, we do not aim to *prove the existence* of a mechanism but rather to document emerging relationships between warming and a set of possible drivers. Further study with *combined observations* and *modeling approaches* is needed.

Acknowledgments
This study was supported by the National Natural Science Foundation of China (41125004), the 111 Project (B14001) and the National Youth Top-Notch Talent Support Program in China. Data to support this article are from the Global Surface Summary of the Day collection archived at the National Climatic Data Center (ftp://ftp.ncdc.noaa.gov/pub/data/qsod), the Monthly Surface Climate Variables of China catalog derived from the National Meteorological Information Center of the China Meteorological Administration (http://cdc.cma.gov.cn), and the Global Historical Climate Network Monthly Version 3 (ftp://ftp.ncdc.noaa.gov/pub/data/ghcn/v3/).

The Editor thanks two anonymous reviewers for their assistance in evaluating this paper.

References

Augustine, J. A., and E. G. Dutton (2013), Variability of the surface radiation budget over the United States from 1996 through 2011 from high-quality measurements, *J. Geophys. Res. Atmos.*, *118*, 43–53, doi:10.1029/2012JD018551.

Beniston, M., and M. Rebetez (1996), Regional behavior of minimum temperatures in Switzerland for the period 1979–1993, *Theor. Appl. Climatol.*, *53*, 231–243.

Beniston, M., H. F. Diaz, and R. S. Bradley (1997), Climatic change at high elevation sites: An overview, *Clim. Change*, *36*, 233–251.
Dominici, F., R. D. Peng, S. L. Zeger, R. H. White, and J. M. Samet (2007), Particulate air pollution and mortality in the United States: Did the risks change from 1987 to 2000?, *Am. J. Epidemiol.*, *166*, 880–888.
Douglass, D. H., B. D. Pearson, and S. F. Singer (2004), Altitude dependence of atmospheric temperature trends: Climate models versus observation, *Geophys. Res. Lett.*, *31*, L13208, doi:10.1029/2004GL020103.
Elvidge, C. D., et al. (2009), Overview of DMSP nighttime lights and future possibilities, *Urban Remote Sensing Event*, *2009 Joint*, (IEEE), pp. 1–5.
Field, C. B., et al. (2014), *Climate Change 2014 Impacts, Adaptation, and Vulnerability: Contribution of Working Group II to the Fifth Assessment Report of the IPCC*, Cambridge Univ. Press, New York.
Fyfe, J. C., and G. M. Flato (1999), Enhanced climate change and its detection over the Rocky Mountains, *J. Clim.*, *12*, 230–243.
Giorgi, F., J. W. Hurrell, M. R. Marinucci, and M. Beniston (1997), Elevation dependency of the surface climate change signal: A model study, *J. Clim.*, *10*, 288–296.
Hansen, J., M. Sato, R. Ruedy, K. Lo, D. W. Lea, and M. Medina-Elizade (2006), Global temperature change, *Proc. Natl. Acad. Sci. U.S.A.*, *103*, 14,288–14,293, doi:10.1073/pnas.0606291103.
Harris, I., P. D. Jones, T. J. Osborn, and D. H. Lister (2014), Updated high-resolution grids of monthly climatic observations—The CRU TS3.10 Dataset, *Int. J. Climatol.*, *34*, 623–642.
Inouye, D. W., B. Barr, K. B. Armitage, and B. D. Inouye (2000), Climate change is affecting altitudinal migrants and hibernating species, *Proc. Natl. Acad. Sci. U.S.A.*, *97*, 1630–1633, doi:10.1073/pnas.97.4.1630.
Kotlarski, S., T. Bosshard, D. Lüthi, P. Pall, and C. Schär (2012), Elevation gradients of European climate change in the regional climate model COSMO-CLM, *Clim. Change*, *112*, 189–215.
Lawrimore, J. H., et al. (2011), An overview of the Global Historical Climatology Network monthly mean temperature data set, version 3, *J. Geophys. Res.*, *116*, D19121, doi:10.1029/2011JD016187.
Li, X. P., L. Wang, D. L. Chen, K. Yang, B. L. Xue, and L. T. Sun (2013), Near-surface air temperature lapse rates in the mainland China during 1962–2011, *J. Geophys. Res. Atmos.*, *118*, 7505–7515, doi:10.1002/jgrd.50553.
Liu, X., Z. Cheng, L. Yan, and Z. Y. Yin (2009), Elevation dependency of recent and future minimum surface air temperature trends in the Tibetan Plateau and its surroundings, *Global Planet. Change*, *68*, 164–174.
Lu, A., S. Kang, Z. Li, and W. Theakstone (2010), Altitude effects of climatic variation on Tibetan Plateau and its vicinities, *J. Earth. Sci.*, *21*, 189–198.
Menon, S., J. Hansen, L. Nazarenko, and Y. Luo (2002), Climate effects of black carbon aerosols in China and India, *Science*, *297*, 2250–2253.
Ohmura, A. (2012), Enhanced temperature variability in high-altitude climate change, *Theor. Appl. Climatol.*, *110*, 499–508.
Pepin, N. C., and M. Losleben (2002), Climate change in the Colorado Rocky Mountains: Free air versus surface temperature trends, *Int. J. Climatol.*, *22*, 311–329.
Pepin, N. C., and J. D. Lundquist (2008), Temperature trends at high elevations: Patterns across the globe, *Geophys. Res. Lett.*, *35*, L14701, doi:10.1029/2008GL034026.
Philipona, R. (2013), Greenhouse warming and solar brightening in and around the Alps, *Int. J. Climatol.*, *33*, 1530–1537.
Rangwala, I., and J. Miller (2012), Climate change in mountains: A review of elevation-dependent warming and its possible causes, *Clim. Change*, *114*, 527–547.
Rangwala, I., E. Sinsky, and J. Miller (2013), Amplified warming projections for high altitude regions of the Northern Hemisphere mid-latitudes from CMIP5 models, *Environ. Res. Lett.*, *8*, 024040, doi:10.1088/1748-9326/8/2/024040.
Rousseeuw, P. J., and A. M. Leroy (2005), *Robust Regression and Outlier Detection*, Wiley, New York.
Ruckstuhl, C., et al. (2008), Aerosol and cloud effects on solar brightening and the recent rapid warming, *Geophys. Res. Lett.*, *35*, L12708, doi:10.1029/2008GL034228.
Santer, B. D., et al. (2005), Amplification of surface temperature trends and variability in the tropical atmosphere, *Science*, *309*, 1551–1556.
Stocker, T. F., et al. (2013), *Climate Change 2013 the Physical Science Basis: Contribution of Working Group I to the Fifth Assessment Report of the IPCC*, Cambridge Univ. Press, New York.
Streets, D. G., et al. (2009), Anthropogenic and natural contributions to regional trends in aerosol optical depth, 1980–2006, *J. Geophys. Res.*, *114*, D00D18, doi:10.1029/2008JD011624.
Vautard, R., P. Yiou, and G. J. van Oldenborgh (2009), Decline of fog, mist and haze in Europe over the past 30 years, *Nat. Geosci.*, *2*, 115–119.
Vestreng, V., G. Myhre, H. Fagerli, S. Reis, and L. Tarrasón (2007), Twenty-five years of continuous sulphur dioxide emission reduction in Europe, *Atmos. Chem. Phys.*, *7*, 3663–3681.
Vuille, M., and R. S. Bradley (2000), Mean annual temperature trends and their vertical structure in the tropical Andes, *Geophys. Res. Lett.*, *27*, 3885–3888, doi:10.1029/2000GL011871.
Wang, K., and R. E. Dickinson (2013), Contribution of solar radiation to decadal temperature variability over land, *Proc. Natl. Acad. Sci. U.S.A.*, *110*, 14,877–14,882, doi:10.1073/pnas.1311433110.
Wang, K., R. E. Dickinson, and S. Liang (2009), Clear sky visibility has decreased over land globally from 1973 to 2007, *Science*, *323*, 1468–1470.
Wang, Q., X. Fan, and M. Wang (2013), Recent warming amplification over high elevation regions across the globe, *Clim. Dyn.*, *43*, 87–101.
Wild, M. (2012), Enlightening global dimming and brightening, *Bull. Am. Meteorol. Soc.*, *93*, 27–37.
Wild, M., et al. (2005), From dimming to brightening: Decadal changes in solar radiation at Earth's surface, *Science*, *308*, 847–850.
Xia, X. (2010), A closer looking at dimming and brightening in China during 1961–2005, *Ann. Geophys.*, *28*, 1121–1132.
You, Q., S. Kang, N. Pepin, W.-A. Flügel, Y. Yan, H. Behrawan, and J. Huang (2010), Relationship between temperature trend magnitude, elevation and mean temperature in the Tibetan Plateau from homogenized surface stations and reanalysis data, *Global Planet. Change*, *71*, 124–133.